

Gradient field microscopy of unstained specimens

Taewoo Kim,¹ Shamira Sridharan,² and Gabriel Popescu^{1,*}

¹Quantitative Light Imaging Laboratory, Department of Electrical and Computer Engineering, Beckman Institute for Advanced Science & Technology, University of Illinois at Urbana-Champaign, Urbana, Illinois 61801, USA

²Quantitative Light Imaging Laboratory, Department of Bioengineering, Beckman Institute for Advanced Science & Technology, University of Illinois at Urbana-Champaign, Urbana, Illinois 61801, USA

*gpopescu@illinois.edu

Abstract: We present a phase derivative microscopy technique referred to as gradient field microscopy (GFM), which provides the first-order derivatives of the phase associated with an optical field passing through a transparent specimen. GFM utilizes spatial light modulation at the Fourier plane of a bright field microscope to optically obtain the derivatives of the phase and increase the contrast of the final image. The controllable spatial modulation pattern allows us to obtain both one component of the field gradient (derivative along one direction) and the gradient intensity, which offers some advantages over the regular differential interference contrast (DIC) microscopy. Most importantly, unlike DIC, GFM does not use polarizing optics and, thus, it is applicable to birefringent samples. We demonstrate these features of GFM with studies of static and dynamic biological cells (HeLa cells and red blood cells). We show that GFM is capable of *qualitatively* providing information about cell membrane fluctuations. Specifically, we captured the disappearance of the bending mode of fluctuations in osmotically swollen red blood cells.

©2012 Optical Society of America

OCIS codes: (170.0180) Microscopy; (170.1530) Cell analysis; (170.1650) Coherence imaging.

References and links

1. G. Popescu, *Quantitative phase imaging of cells and tissues* (McGraw-Hill, 2011).
2. "Milestones in light microscopy," *Nat. Cell Biol.* **11**(10), 1165–1165 (2009).
3. F. Zernike, "How I discovered phase contrast," *Science* **121**(3141), 345–349 (1955).
4. M. G. Nomarski, "Microinterferometre differentiel a ondes polarisees," *J. Phys. (Paris)* **16**, S9–S13 (1955).
5. D. K. Hamilton and C. J. R. Sheppard, "Differential phase-contrast in scanning optical microscopy," *J Microsc. (Oxford)* **133**(1), 27–39 (1984).
6. T. Wilson, "Enhanced differential phase-contrast imaging in scanning microscopy using a quadrant detector," *Optik (Stuttg.)* **80**, 167–170 (1988).
7. A. Ahn, C. H. Yang, A. Wax, G. Popescu, C. Fang-Yen, K. Badizadegan, R. R. Dasari, and M. S. Feld, "Harmonic phase-dispersion microscope with a Mach-Zehnder interferometer," *Appl. Opt.* **44**(7), 1188–1190 (2005).
8. C. H. Yang, A. Wax, I. Georgakoudi, E. B. Hanlon, K. Badizadegan, R. R. Dasari, and M. S. Feld, "Interferometric phase-dispersion microscopy," *Opt. Lett.* **25**(20), 1526–1528 (2000).
9. C. K. Hitzenberger and A. F. Fercher, "Differential phase contrast in optical coherence tomography," *Opt. Lett.* **24**(9), 622–624 (1999).
10. M. Lew, X. Q. Cui, X. Heng, and C. H. Yang, "Interference of a four-hole aperture for on-chip quantitative two-dimensional differential phase imaging," *Opt. Lett.* **32**(20), 2963–2965 (2007).
11. C. Rylander, T. E. Milner, K. R. Diller, and A. J. Welch, "Spatial refractive index determination of single cells using differential phase optical low-coherence reflectometry," *Lasers Surg. Med.*, 5–5 (2003).
12. T. J. McIntyre, C. Maurer, S. Bernet, and M. Ritsch-Marte, "Differential interference contrast imaging using a spatial light modulator," *Opt. Lett.* **34**(19), 2988–2990 (2009).
13. S. H. Lee and D. P. Casasent, *Optical Information Processing: Fundamentals* (Springer-Verlag, 1981).
14. T. Kim and G. Popescu, "Laplace field microscopy for label-free imaging of dynamic biological structures," *Opt. Lett.* **36**(23), 4704–4706 (2011).
15. W. C. Stewart, "Differential phase-contrast with an extended illumination source," *J. Opt. Soc. Am.* **66**(8), 813–818 (1976).

16. B. Kachar, "Asymmetric illumination contrast: a method of image formation for video light microscopy," *Science* **227**(4688), 766–768 (1985).
17. S. B. Mehta and C. J. R. Sheppard, "Quantitative phase-gradient imaging at high resolution with asymmetric illumination-based differential phase contrast," *Opt. Lett.* **34**(13), 1924–1926 (2009).
18. R. Yi, K. K. Chu, and J. Mertz, "Graded-field microscopy with white light," *Opt. Express* **14**(12), 5191–5200 (2006).
19. G. Popescu, K. Badizadegan, R. R. Dasari, and M. S. Feld, "Observation of dynamic subdomains in red blood cells," *J. Biomed. Opt.* **11**(4), 040503 (2006).
20. G. Popescu, T. Ikeda, K. Goda, C. A. Best-Popescu, M. Laposata, S. Manley, R. R. Dasari, K. Badizadegan, and M. S. Feld, "Optical measurement of cell membrane tension," *Phys. Rev. Lett.* **97**(21), 218101 (2006).
21. H. F. Ding, Z. Wang, F. Nguyen, S. A. Boppart, and G. Popescu, "Fourier transform light scattering of inhomogeneous and dynamic structures," *Phys. Rev. Lett.* **101**(23), 238102 (2008).
22. Y. K. Park, C. A. Best, T. Auth, N. S. Gov, S. A. Safran, G. Popescu, S. Suresh, and M. S. Feld, "Metabolic remodeling of the human red blood cell membrane," *Proc. Natl. Acad. Sci. U.S.A.* **107**(4), 1289–1294 (2010).
23. Y. K. Park, C. A. Best, K. Badizadegan, R. R. Dasari, M. S. Feld, T. Kuriabova, M. L. Henle, A. J. Levine, and G. Popescu, "Measurement of red blood cell mechanics during morphological changes," *Proc. Natl. Acad. Sci. U.S.A.* **107**(15), 6731–6736 (2010).
24. Y. Park, C. A. Best, T. Kuriabova, M. L. Henle, M. S. Feld, A. J. Levine, and G. Popescu, "Measurement of the nonlinear elasticity of red blood cell membranes," *Phys. Rev. E Stat. Nonlin. Soft Matter Phys.* **83**(5), 051925 (2011).
25. Y. K. Park, M. Diez-Silva, G. Popescu, G. Lykotrafitis, W. S. Choi, M. S. Feld, and S. Suresh, "Refractive index maps and membrane dynamics of human red blood cells parasitized by *Plasmodium falciparum*," *Proc. Natl. Acad. Sci. U.S.A.* **105**(37), 13730–13735 (2008).
26. N. Gov, A. G. Zilman, and S. Safran, "Cytoskeleton confinement and tension of red blood cell membranes," *Phys. Rev. Lett.* **90**(22), 228101 (2003).

1. Introduction

Unlabeled biological cells and tissues are mostly transparent under visible light due to the very low absorption and weak scattering. Therefore, they can be assumed as phase objects with a transmission function of the form $t(x, y) = A \exp[i\phi(x, y)]$ [1]. Since the bright field microscopy measures the intensity of the field, the phase information which gives the intrinsic contrast is lost at the detector and no contrast is obtained for phase objects with constant amplitude, i.e., $|t|^2 = A^2$. During its four-century long history, much of the microscopy development has been focused on finding modalities to achieve higher contrast [2]. *Exogenous contrast*, obtained by adding chemical compounds (e.g. dyes, fluorophores, or nanoparticles), has been developed essentially to turn a phase object into an amplitude object and, thus, obtain higher contrast. On the other hand, *intrinsic contrast* methods have been developed to use the existing information carried by the light passing through the transparent samples, without using contrast agents. These intrinsic contrast methods are valuable because of their non-invasive and label-free nature, which allows us to study the biological specimens unperturbed.

Along with Zernike's Phase contrast (PC) microscopy [3], Nomarski's differential interference contrast (DIC) microscopy [4] has been one of the most commonly used techniques for intrinsic contrast imaging [5–11]. DIC qualitatively provides the first-order derivative of the phase through interference of two identical but laterally shifted fields. Thus, the images obtained by DIC are very sensitive to the edges and changes in the sample. However, because of the rapid sign changes of the first-order derivatives at the edges or the samples, DIC suffers from the directional shadow artifact in the direction of the shift. Also, since DIC utilizes polarization optics, birefringent materials cannot be readily investigated.

Here, we introduce a new method referred as gradient phase microscopy (GFM), based on the spatial filtering of light at the back focal plane of the objective [12–14]. This method carries the spirit of DIC by providing the first-order derivative of the phase while overcoming these two limitations of conventional DIC: the directional shadow artifact and the incapability of using birefringent samples. The former obstacle is overcome by measuring the gradient amplitude (intensity) rather than one of its components. We met the latter challenge by using

spatial light modulation without polarizing optics to achieve interference between two shifted replicas of the image field.

2. GFM setup

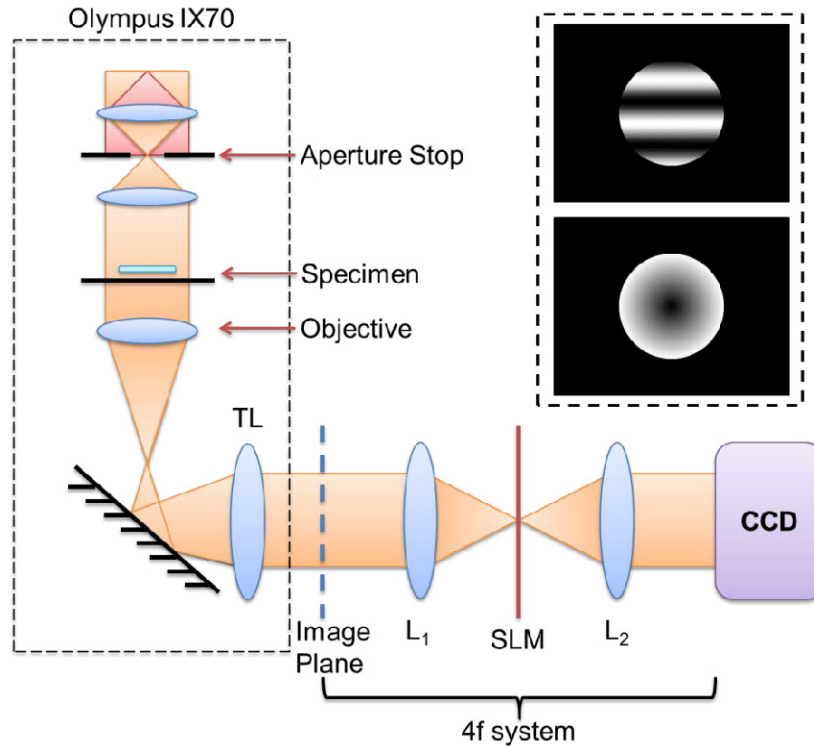


Fig. 1. GFM setup: L1 and L2 have focal length of 75mm and 150mm, respectively. The spatial light modulator (SLM) with contrast ratio of 400/1 and pixel size $13\mu\text{m}$ is obtained from Epson Powerlite S5 commercial projector. Andor iXon + EMCCD is used for the detection. Inset: modulation filters projected on SLM for sine-GFM (top) and linear-GFM (bottom).

A schematic of the GFM setup is shown in Fig. 1. GFM is built as an add-on module to the output port of an otherwise unmodified commercial microscope (Olympus IX70). The white light illumination from a halogen lamp is filtered through the aperture stop to provide high spatial coherence of the illumination. The transmitted and scattered light from the sample is collected by the objective lens, and forms an image through the tube lens (TL). At the image plane of the microscope, the GFM setup starts by forming a $4f$ imaging system including two lenses and an amplitude-only spatial light modulator (SLM). The liquid crystal SLM is obtained from an Epson Powerlite S5 projector with a contrast ratio of 400/1 and pixel size $13\mu\text{m}$. This pixel size limits the resolution in k -space, δk , which indicates the field of view at the image plane over which the modulation produced by one SLM pixel is uniform. With 150mm focal length lens, this uniformly modulated field of view in the image plane is of the order of 6.25mm. We were able to obtain high contrast images over the entire CCD area, which is a square with 13mm sides. The Fourier transform of the image formed at the image plane is generated through lens L_1 which locates at a focal distance away from the image plane. The SLM provides a variable amplitude filter at the Fourier plane, and lens L_2 takes the Fourier transform of the modulated spatial frequency map back to the image (CCD) plane. The inset of Fig. 1 shows the two modulation patterns used at the Fourier plane in our setup to obtain 1D phase derivative (top) and gradient intensity (bottom). The modulation on the top is

a sine function in the y -direction of the spatial frequency domain, $H(k_x, k_y) = A[1 + \sin(ak_y)]$. This modulation generates two shifted duplicates of the field, which then interfere and form the first-order derivative of the field as

$$\begin{aligned} [1 + \sin(ak_y)]U(k_x, k_y) &\leftrightarrow \left[\delta(x, y) + \frac{\delta(x, y - a) - \delta(x, y + a)}{2i} \right] * U(x, y) \\ &= U(x, y) + ia \frac{\partial U(x, y)}{\partial y} \end{aligned} \quad (1)$$

In Eq. (1), a , $k_{x,y}$, and $U(x,y)$ are the inverse period of the sine modulation, spatial frequencies in x and y direction, and the scattered field at the image plane of the microscope, respectively. Therefore, for a purely phase object (of unit amplitude), $U(x, y) = \exp[i\phi(x, y)]$, we obtain the first order derivative of the phase at the image plane along with some DC component.

$$I(x, y) = \left| e^{i\phi(x,y)} - a \frac{\partial \phi(x, y)}{\partial y} e^{i\phi(x,y)} \right|^2 \approx 1 - 2a \frac{\partial \phi(x, y)}{\partial y} \quad (2)$$

In Eq. (2), $I(x,y)$ and $\phi(x,y)$ represent the measured intensity at the detector and the phase of the scattered field, respectively. As shown in Eq. (2), this sine-modulation GFM gives the identical result as the regular DIC. Note that, unlike in DIC, where birefringent prisms are used to generate the two interfering beams, GFM operates without polarization optics. Thus, the GFM add-on can be used with a regular bright field microscope, without the need for specialized optics. Using a grating filtering at the back focal plane of the objective to generate a gradient image has also been demonstrated by McIntyre *et al.* [12] by taking the two first-order diffracted field, shifted with two different distance from the DC field because of the two different grating periods. Compared to this method, our sine-GFM exhibits lower loss of light, since it uses the DC component and the positive and negative shifted first-order diffracted fields. Consequently, this advantage enables sine-GFM to be used with shorter exposure time which provides the ability to measure dynamic specimen. Furthermore, the use of white light instead of a laser reduces speckle and provides higher resolution in the images.

In order to obtain the intensity of the gradient, we use a ‘‘cone-like’’ filter shape, $H(k_x, k_y) = (k_x^2 + k_y^2)^{1/2} = |k_r|$. The measurement at the detector gives us the square of the first-order derivative of the phase as

$$I(r) = \left| FT \left[|k_r| U(k_r) \right] \right|^2 \approx \left| \frac{\partial \phi(r)}{\partial r} \right|^2, \quad (3)$$

where I is the intensity measured at the CCD. The advantage of this linear modulation is that there is no directional shadow artifact that occurs in DIC due to the rapidly changing sign of the derivative. However, in Eq. (3), the derivative image obtained from this linear modulation assumes that the field is rotationally symmetric. The image may be degraded for specimens without such symmetry. Thus, in practice one can chose between the two complementary methods (sine- and linear-GFM) according to the properties of the sample, or combine multiple modes of GFM to obtain the full vector gradient of the phase of the sample, e.g. combining two sine-GFM images with shifts in different directions. However, we do not see a significant practical advantage in doing so for the specimen presented, so only one mode is used at a time in this manuscript.

3. Live cell imaging using GFM

In order to test the ability of GFM to generate high-contrast images of transparent samples, measurements on unlabeled HeLa cells were made. HeLa cells were prepared at 30% confluency in a 35mm glass bottom dish (MatTek, P35G-1.0-14-C, uncoated) with EMEM(ATCC, 30-2003) with 10% FBS (ATCC, 30-2020). The passaged cells then were left in the incubator for a day at 37°C and 5% CO₂ concentration in a humidified environment, so that they can attach and flatten to the bottom of the dish. Since the switching among BF, linear-GFM and sine-GFM are done by simply changing the modulation pattern on the SLM, measurement on the very same field of view is made possible, which provides us with a direct comparison between the methods. Figures 2(a)-2(c) show images of HeLa cells under BF, linear-GFM and sine-GFM, respectively. For the cells that are well-attached to the bottom of the dish, the contrast in BF is extremely low. Clearly, these cells become much more visible under linear-GFM with no directional artifact, and sine-GFM with y-directional artifact.

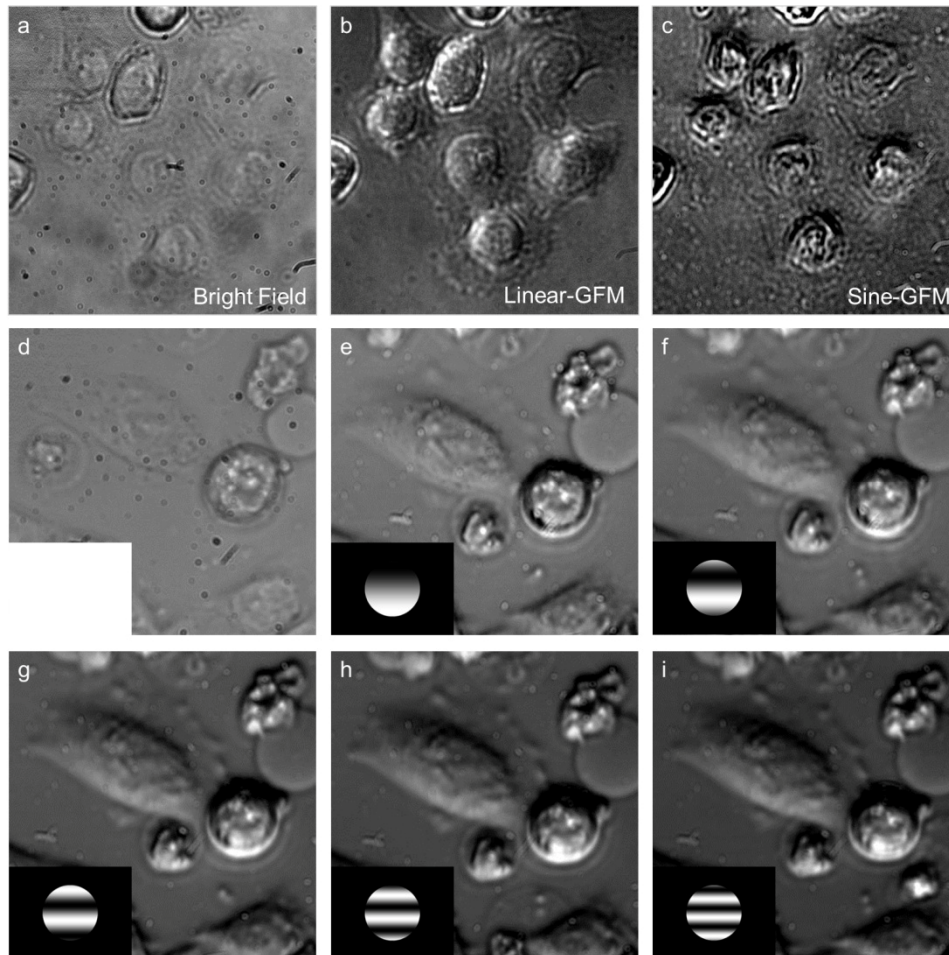


Fig. 2. Same HeLa cells under (a) bright field, (b) linear-GFM, and (c) sine-GFM;40x, 0.6NA objective. (d)-(i) HeLa cells imaged with different period sine modulation All images are taken using a 40x, 0.6NA objective. Insets of (d)-(i) show the modulation filters used for the HeLa cell image. (Media 1) The movie contains another field of view in the HeLa cell sample with varying filter period.

One important feature of sine-GFM is that the shift amount can be controlled easily to provide the highest contrast. Figures 2(d)-2(i) show the same HeLa cell imaged by GFM with six different sine modulations. The inset of each image represents the filter that is projected on the SLM; of course, the filter in Fig. 2(d) gives an image identical to that in BF image since there is no modulation given at the Fourier plane. As the period of the sine modulation gets smaller (larger shift in the image plane), we can see more of the overall shape of the cells, i.e., low-frequency component. Conversely, for larger sine periods, small details become more visible. This result shows that sine-GFM can be used for objects of many different scales.

4. GFM using birefringent substrates

Regular DIC uses Wollaston prisms, which prevents imaging birefringent specimens or specimens on birefringent substrates such as plastic. Therefore, for regular DIC imaging of biological cells and tissues, glass bottom dishes or glass slides must be used to avoid this birefringence effect. Different methods for birefringence-immunity in getting phase-gradient images have been suggested [15–18], and here, we also suggest the birefringence-immunity of our GFM system. Since GFM is built as a module that starts at the image plane of a bright field microscope, it can generate a derivative field as long as the correct image can be formed at the image plane.

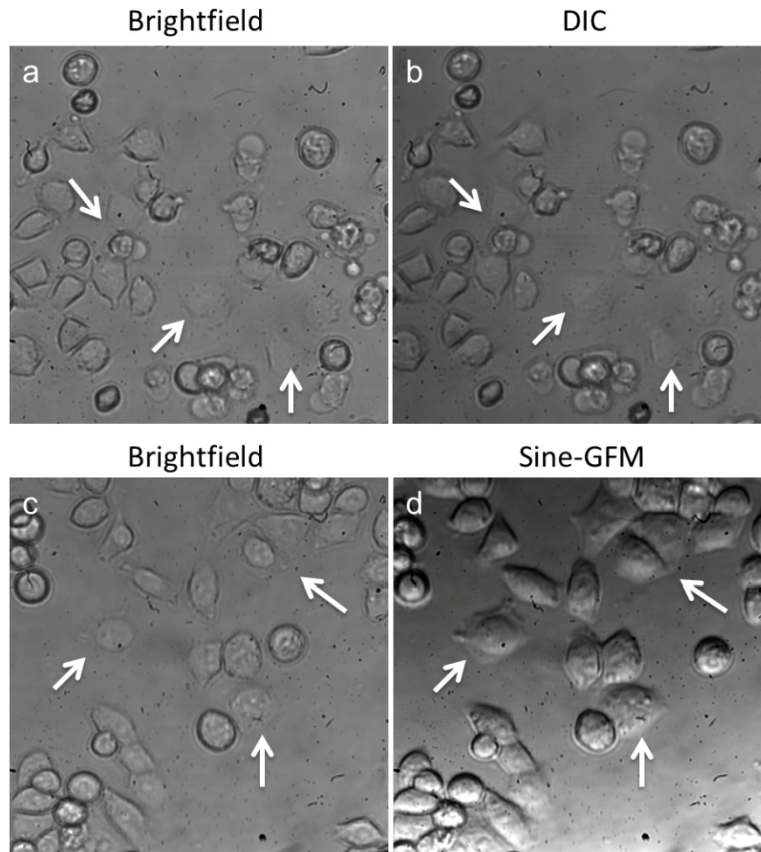


Fig. 3. (a)-(b) comparison between BF and commercially available DIC on the same field of view, indicating a modest increase in contrast. (c)-(d) Comparison between BF and sine-GFM at the same field of view. Evident contrast enhancement is observed for the cells indicated by arrows.

Figure 3 shows HeLa cells imaged in plastic petri dishes using a 40x, 0.6NA objective. Figures 3(a) and 3(b) show the comparison between the bright field and the regular DIC imaging performance under the presence of plastic petri dish. Notice the cells indicated by the white arrows show very low contrast in both BF and DIC, which shows the limitations of DIC when birefringent materials are used. Figures 3(c) and 3(d) show the comparison between BF and GFM, again for HeLa cells using a plastic petri dish. Looking at the cells indicated by the arrows, it is very clear that GFM increases the contrast of phase objects even when birefringent substrates are used. Although there is a cost of resolution that comes from smaller condenser aperture compared to commercial DIC, GFM provides a solution for situations when DIC is not effective, like, for example, when the substrate is birefringent. This capability of using birefringent materials in DIC imaging not only expands the variety of usable materials, but also brings more cost-efficiency to DIC imaging since the plastic containers used in microscopy imaging are usually much less expensive than the glass containers.

5. Red blood cell dynamics

One valuable feature of sine-GFM is its measurement speed. Compared to linear-GFM, the light power lost through the SLM is significantly lower for sine-GFM and, as a result, it allows measurements under shorter exposure time and higher acquisition rate. In fact, sine-GFM can acquire images as fast as the camera acquisition speed since there is no need for additional image processing. Therefore, sine-GFM is suitable for studying dynamic samples such as biological cells. Since sine-GFM measures the first-order derivative of the phase, it is very sensitive to fluctuations where there is a rapid change of the field. In particular, GFM can detect nanoscale motions of red blood cell (RBC) membranes. These fluctuations have been studied actively in the past few years both for their interesting dynamics, at the basic science level [19–24], and their potential for diagnosing disease at a single cell level [25].

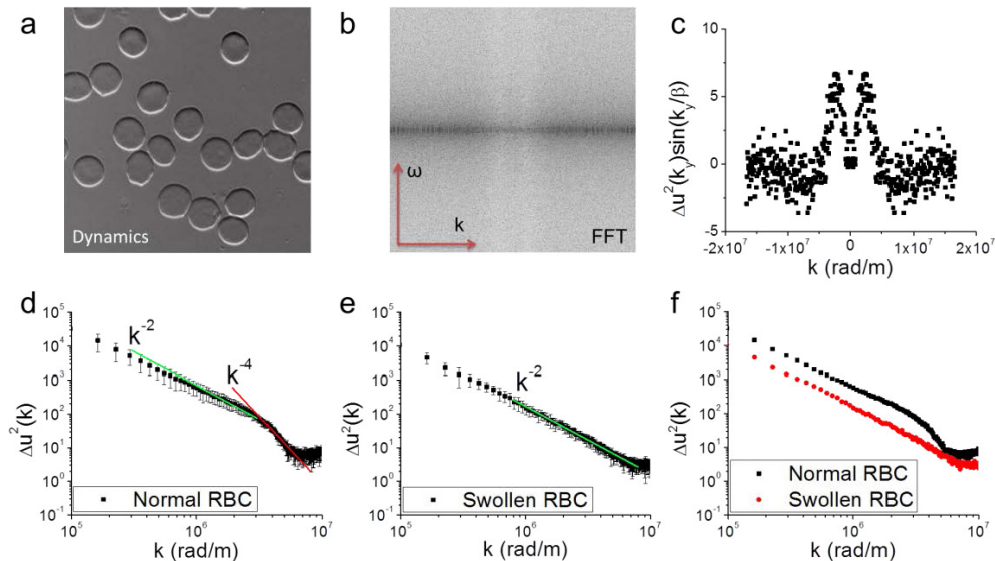


Fig. 4. Dynamic measurement of red blood cell (RBC) membrane fluctuations. (Media 2) The movie shows a time-lapse measurement of a blood smear sample. (a) One frame from a time-lapse measurement of a blood smear on a glass slide imaged by sine-GFM. (b) 2D (space-time) power spectrum associated with the time-lapse displacement. (c) spatial power spectrum that shows the sine function applied by the SLM. (d) MSD vs. k after sine removal, for normal RBCs (errors indicated standard deviation for $N = 20$ cells). k^{-2} and k^{-4} power laws are indicated as a green and red line, respectively. (e) MSD vs. k for osmotically swollen

spherocyte (errors indicated standard deviation for $N = 20$ cells). k^{-2} power law is indicated as a green line. (f) comparison between the average MSDs for the normal and swollen RBCs.

In previous studies, the dynamics of RBC membrane fluctuation has been studied in terms of the relationship between the spatial frequency, k , and the mean-square displacement (MSD) of the RBC membrane, $\Delta u^2(k)$ [26].

$$\Delta u^2(k) = \frac{k_B T}{\kappa k^4 + \sigma k^2} \quad (4)$$

In Eq. (4), k_B is the Boltzmann constant, T the absolute temperature, κ the membrane bending modulus, and σ the apparent tension coefficient. Later, it was found that the physical origin of the tension mode is the coupling between compression and bending modes [23]. From the equation, it is expected that the MSD of the membrane depends on k^{-2} at low spatial frequencies and on k^{-4} at high spatial frequencies.

We used sine GFM to measure the spatial power spectrum, $\Delta u^2(k)$. The spatial power spectrum of the sine-GFM image is, to a good approximation, $\sin(ak_y) |U(k_x, k_y)|^2$, as obtained by taking the modulus squared of Eq. (1) and ignoring the \sin^2 term. Thus, to obtain the MSD, we need to remove the (known) sinusoid. Figure 4 shows this procedure and the result of RBC membrane dynamics under sine-GFM. Blood smeared on a glass slide was imaged using 100x, 1.4NA oil immersion objective. The image acquisition was performed with Andor iXon⁺ EMCCD using 2-by-2 binning, which yielded an acquisition rate of 8 frames per second. Figure 4(a) shows one frame of the time-lapse stack of RBC sine-GFM images. In order to get a spatiotemporal power spectrum, we took the 3D power spectrum of our time-resolved images and resliced it to show the spatial frequency along the modulation direction (k_y) and temporal frequency, ω . This ω - k_y domain image, Fig. 4(b), contains full information about the spatiotemporal fluctuations of RBC membranes. By taking the average over ω , the MSD modulated by the sine is obtained (Fig. 4(c)). Since this sine function is due to the SLM filter, it is known and can be removed numerically via a simple division. Figure 4(d) shows the resulting MSD for normal discocyte RBCs, where the expected k^{-2} and k^{-4} power laws are obtained. We prepared a sample of osmotically swollen cells and studied the differences between the two fluctuation power spectra. Figure 4(e) shows the MSD for swollen, *spherocyte* RBCs prepared by adding water to the blood smear. Both plots are obtained by averaging over 20 measurements and the error bars represent the standard deviation. In Fig. 4(f), we show a comparison between the dynamics of discocyte and spherocyte cells. Interestingly, we found that for spherocytes, the k^{-2} power law behavior is shown to exist at high frequencies as well which is an indication that the bending mode is subdominant throughout the entire spatial domain. This finding is consistent with recent studies performed by quantitative phase imaging, where the spatial correlations associated with the membrane fluctuations appeared narrower for swollen cells.

Remarkably, our results show that useful information can be retrieved from nanoscale fluctuations using only a derivative of the phase and not the phase itself. This is quite a general result, i.e., similar information as in Figs. 4(d) and 4(e) can be obtained using a commercial DIC microscope. This type of measurement is much more easily implemented than a quantitative phase imaging method (see Ref [1]. for a review of such methods). However, the price we pay for not using full (*quantitative*) phase information is the lack of *quantitative* statements we can make about the mechanical parameters of the membrane, e.g., κ and σ . In other words, using the gradient images to calculate the power spectra, there is no method to normalize the curves (e.g., Fig. 4(e)). Thus, we cannot *fit* the curve to extract quantitatively the parameters. If quantitative information is the goal, one should use instead quantitative phase imaging, as shown in Refs [1, 20–25].

6. Summary

A new first-order phase derivative microscopy technique referred to as gradient field microscopy (GFM) was introduced as an efficient method to generate contrast of transparent samples. GFM is built as an outside module attached to a commercial bright field microscope. Significant increase in contrast was observed when imaging cells in plastic dishes with GFM compared to the conventional bright field microscope and commercial differential interference contrast (DIC) microscopy. While maintaining the contrast, GFM successfully removes the directional shadow artifact by generating the intensity of the phase gradient. Finally, for the first time to our knowledge, we show that phase derivatives and, hence, GFM can inform about dynamics of cell membranes and reveal, for example, the dominant modes of deformation. This feature has potential applications both in basic science and clinical diagnosis of blood.

Acknowledgments

This research was supported by the National Science Foundation (grants CBET 08-46660 CAREER, CBET-1040462 MRI) and National Cancer Institute (R21 CA147967-01). TK and SS acknowledge help with HeLa cell preparation from Ryan Tapping. For more information, visit <http://light.ece.illinois.edu/>.